SF2A 2024
M. Béthermin, K. Baillié, N. Lagarde, J. Malzac, R.-M. Ouazzani, J. Richard, O. Venot, A. Siebert (eds)

EXPLORING THE SUBTLETIES OF FEEDBACK PROCESSES THROUGH THE CGM IN GALAXY SIMULATIONS

M. Rey[1], J. Blaizot[2], T. Kimm[1], J. Rosdahl[2] and L. Michel-Dansac[3]

Abstract. Numerical simulations have become an essential tool in modern astrophysical research, greatly improving our understanding of the complex processes that govern galaxy formation and evolution. However, their complexity and computational expense necessitate subgrid models for star formation and stellar feedback which, although capable of reproducing various observations, are inherently non-unique and subject to degeneracy. To differentiate between competing models, we investigate the potential of quasar absorption lines of the circumgalactic medium (CGM). To that aim, we run three simulations of the same galaxy with RAMSES-RT, using three common subgrid models. We first calibrate the stellar masses of simulated galaxies at redshift $z = 1$ and post-process with KROME and RASCAS to obtain their respective H I, Mg II, C IV, and O VI radial column density. Our analysis reveals distinct properties and feedback mechanisms across the three models, with variations in the CGM properties highlighting the degeneracy inherent in the subgrid prescriptions. All three models struggle to reproduce observed cold gas column densities (H I and Mg II). For warm and hot gas tracers (C IV and O VI), the delayed cooling model exhibits much better agreement than the two others thanks to more efficient metal ejection from the galaxy into the CGM.

Keywords: methods: numerical, galaxies:evolution, quasars: absorption lines

1 Introduction

In recent years, numerical simulations have become essential for predicting and interpreting astrophysical observations. They are particularly powerful for studying galaxy formation and evolution as they enable the analysis of complex systems across a vast range of scales and physical processes. Simulations rely on *subgrid models* to describe physics below the resolution limit, for example, star formation and stellar feedback. Many models have been developed (Vogelsberger et al. 2020) and have proven successful in reproducing various observables (Crain & van de Voort 2023). However, models motivated by entirely different physical principles can simultaneously match observational constraints. Therefore, it is crucial to identify strong complementary constraints to differentiate these models. The circum-galactic medium (CGM) surrounds the galaxy and hosts both inflows from the cosmic web and outflows from the galaxy. These complex dynamics and multiphase nature makes it challenging to model in simulations. In parallel, our understanding of this medium has significantly improved in the last decade, notably thanks to HST-COS (Faucher-Giguère & Oh 2023). New instruments such as DESI (Chang et al. 2024) will push our understanding of this medium further, allowing us to interpret observations with the help of simulations. In this work, we demonstrate how the CGM can provide a strong constraint to differentiate subgrid models, thus improving current simulations and our understanding of the galactic baryon cycle.

2 Three zoom simulations of the same galaxy

The numerical setup is fully detailed in Rey et al. (in prep.). In brief, we perform zoom cosmological radiative hydrodynamics simulations using the adaptive mesh refinement code RAMSES-RT (Teyssier 2002,

[1] Department of Astronomy, Yonsei University, 50 Yonsei-ro, Seodaemun-gu, Seoul 03722, Republic of Korea
[2] Centre de Recherche Astrophysique de Lyon, UMR5574, Université Claude Bernard Lyon 1, ENS de Lyon, CNRS, 9 av. Charles André, F-69230 Saint-Genis-Laval, France
[3] Aix Marseille Univ., CNRS, CNES, LAM, Marseille, France

Rosdahl & Teyssier 2015). We model the evolution of gas and radiation as fluids (maximal resolution of $\Delta x \approx 40\,\mathrm{pc}$), and dark matter and stars as collisionless particles (respective resolution of $\mathrm{m_{DM,min}} = 3.47 \times 10^5\ \mathrm{M_\odot}$ and $\mathrm{m_{\star,min}} = 3.2 \times 10^4\ \mathrm{M_\odot}$). We trace all hydrogen and helium ionisation states, and track metals through the metal mass fraction Z. We use MUSIC (Hahn & Abel 2011) to generate zoom initial conditions, targeting a halo of mass $\mathrm{M_{halo}} = 5.33 \times 10^{11}\mathrm{M_\odot}$ at $z = 0$ in a $30\,\mathrm{cMpch^{-1}}$ box. We then model the evolution of this galaxy down to redshift $z = 1$ with three subgrid models commonly used in the literature, we refer to them as KI (Kimm et al. 2017), KR (Kretschmer & Teyssier 2020) and DC (Teyssier et al. 2013). All three runs rely on a multi-freefall star formation model, but KR additionally models turbulence through a subgrid model. KI models feedback by injecting momentum in the surrounding media based on high-resolution simulations whereas KR switches between momentum and thermal feedback depending on the resolution, and DC uses delayed cooling. We also calibrate the three simulations in stellar mass to assess the potency of CGM observables as *additional* constraints to galactic properties.

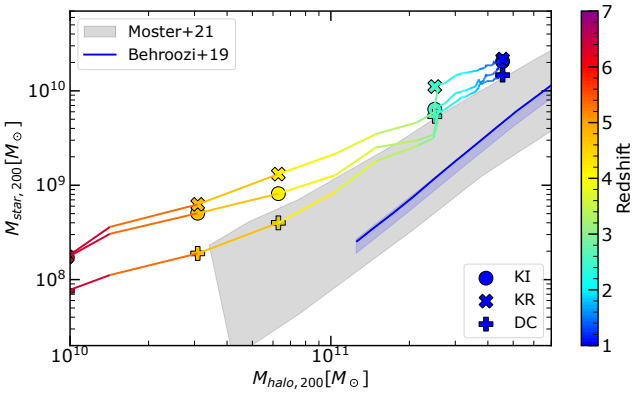

Fig. 1: Stellar mass to halo mass relation for the KI, KR and DC simulations. Distinct markers denote the three simulations, and we colour the curves with redshift. The solid blue line shows the relation derived by Behroozi et al. (2019) at $z = 1$, with its 16^{th}–84^{th} percentiles shown by the shaded area. The grey-shaded region shows reinforced learning predictions from Moster et al. (2021). By z=1, the three simulations converge to a similar stellar mass, albeit slightly exceeding observational expectations

Fig. 1 shows the stellar mass to halo mass relation of the KI, KR and DC simulations. We compute the stellar mass as the mass within $0.1\mathrm{R_{vir}}$, with $\mathrm{R_{vir}}$ the virial radius. The halo mass is taken from a twin dark matter-only simulation. Although the trajectory of DC is different than KI and DC at redshift $z \gtrsim 4$, the three simulations converge by redshift $z = 1$ to $\mathrm{M_{\star,KI}} = 2.05 \times 10^{10}\,\mathrm{M_\odot}$, $\mathrm{M_{\star,KR}} = 2.17 \times 10^{10}\,\mathrm{M_\odot}$, and $\mathrm{M_{\star,DC}} = 1.47 \times 10^{10}\,\mathrm{M_\odot}$ for a dark halo mass of $M_{\star,200} = 4.6 \times 10^{11}\,M_\odot$. Although the mass of the three galaxies is slightly higher than the expected relation, we caution that these comparisons are indirect and both observation and simulations suffer from uncertainties, e.g. through the stochasticity of star formation (Keller et al. 2019; Genel et al. 2019). Nonetheless, our goal of producing galaxies with similar stellar masses is reached.

3 Impact of subgrid models on the CGM

Before looking at CGM observables, we show quantitative key differences between the three simulations, and how their feedback mechanisms differ. Fig. 2 shows density and metallicity maps of the three simulations at $z = 1$. By eye, we can already see that the gas density in the CGM is higher in both KI and DC than in KR. We confirm this by computing the baryon mass fraction (i.e. gas + stars) in the CGM which is 34% and 33% for KI and DC, and only 9% for KR. We also find that even though the stacked total halo masses are similar ($M_\mathrm{b} = 3.63 - 3.79 \times 10^{11}\,\mathrm{M_\odot}$), the halo baryonic mass is higher in KI ($M_\mathrm{b} = 4.44 \times 10^{10}\,\mathrm{M_\odot}$) than in KR ($M_\mathrm{b} = 3.22 \times 10^{10}\,\mathrm{M_\odot}$) and DC ($M_\mathrm{b} = 2.94 \times 10^{10}\,\mathrm{M_\odot}$). This shows that KR and DC are more efficient in regulating baryons on large scales, through either ejective or preventive feedback. Within the halo, the difference between KR and DC is that while KR keeps most halo baryons in stars, a significant fraction of these baryons is ejected in the CGM with DC. If we now look at the metallicity of the gas, we find that KR and DC both show high-metallicity gas in the CGM gas while the CGM gas in KI has a relatively low metallicity. Overall, we thus find that the three different models lead to distinct feedback mechanisms. These differences result in a CGM which is gas-rich with low metallicity in KI, gas-poor with high metallicity in KR, and gas-rich with high metallicity in DC.

Having seen that the baryon cycle differs among the three models, we now compare our simulations to CGM observables. To that aim, we first estimate the Mg, C and O number densities from the metallicity of the simulation, assuming solar abundances of $A_{\mathrm{Mg},\odot} = 3.98 \times 10^{-5}$, $A_{\mathrm{C},\odot} = 2.69 \times 10^{-4}$ and $A_{\mathrm{O},\odot} = 4.9 \times 10^{-4}$ (Grevesse et al. 2010). Then, by evolving the ionisation balance to equilibrium (Mauerhofer 2021) with KROME (Grassi et al. 2014) we obtain Mg II, C IV, and O VI ionisation fractions. Lastly, we integrate the density along 10^5

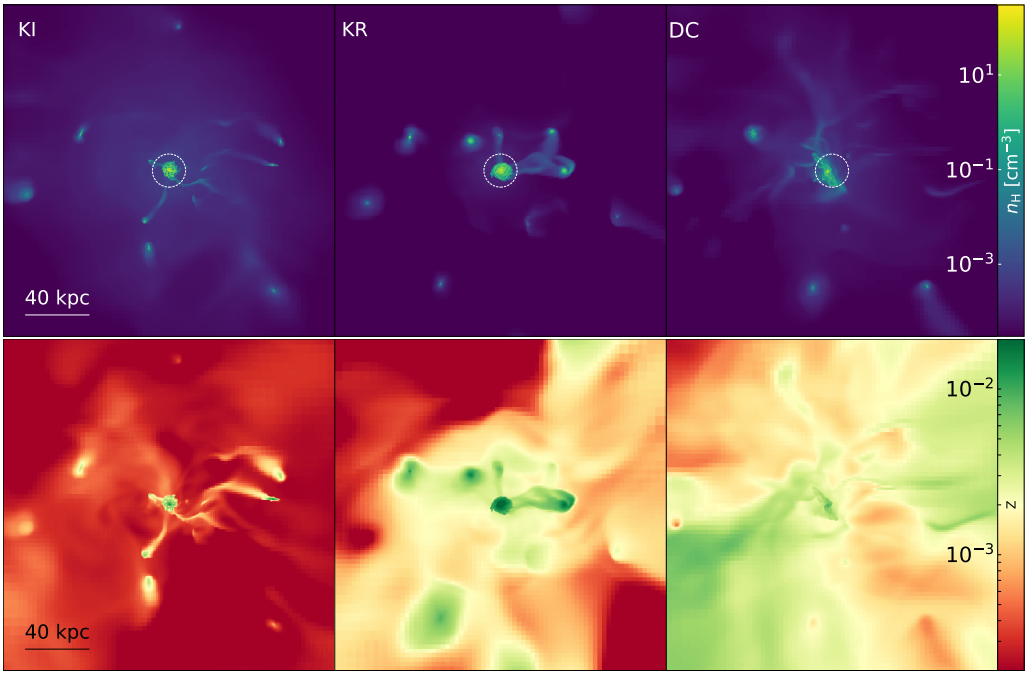

Fig. 2: Density-weighted projections of density (top) and metallicity (bottom) of the galaxy at $z = 1$ for KI, KR, and DC (from left to right). This plot illustrates how the KI and DC simulations have more baryons in their CGM while the metallicity of the gas is higher in KR and DC.

lines of sight spanning $5R_{vir}$ in random directions crossing the CGM at impact parameters uniformly sampled up to $2R_{vir}$ with RASCAS (Michel-Dansac et al. 2020) to obtain column densities.

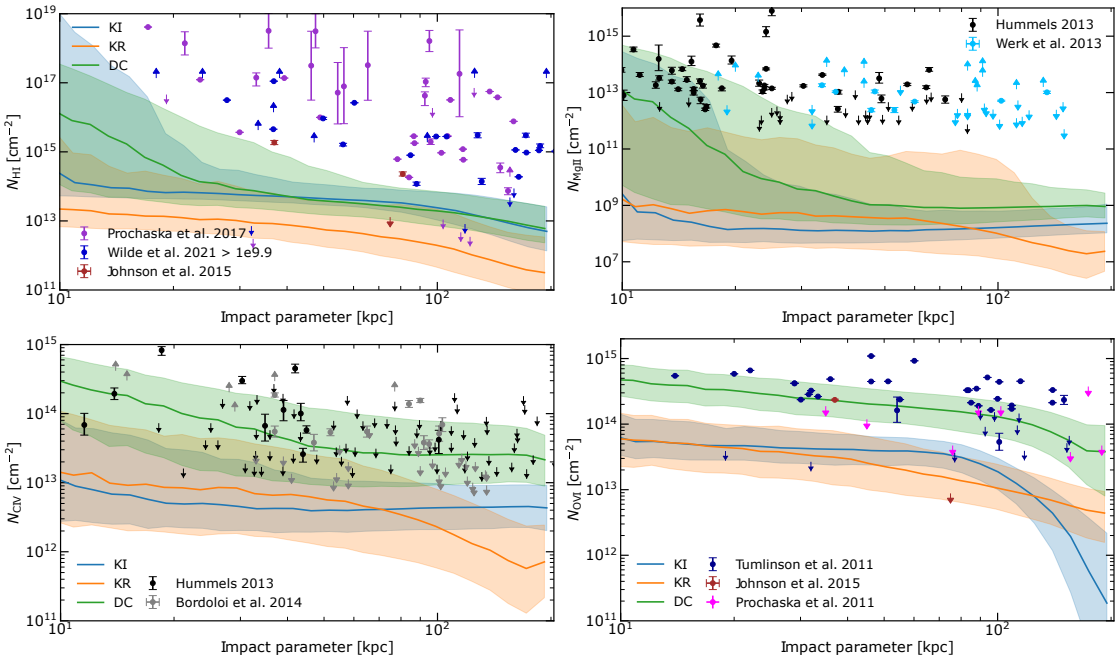

Fig. 3: Column density of H I, Mg II, C IV, and O VI (from top-left to bottom right) as a function of impact parameter. KI (blue), KR (orange) and DC green) are shown by solid lines, and markers denote observations. KI and KR struggle to match any observational constraints, while DC is in better agreement with observations for C IV, and O VI.

Fig. 3 shows the radial column density of H I, Mg II, C IV, and O VI for three simulations, also stacked over

1 Gyr, from $z = 1.3$ to $z = 1$. Focusing first on comparing models, we find that we can discriminate KI, KR and DC through the chosen ions. In H I, both KI and DC exhibit similar column densities while column densities for DC are higher in Mg II. This is a direct consequence of the different properties of the CGM seen in Fig. 2. While KI and DC have a comparable gas mass in the CGM (i.e. similar H I column densities), the metallicity of this gas is higher in DC, and so are the simulated Mg II column densities. Similarly, KI is higher than KR in H I due to a higher CGM gas mass, but comparable in Mg II. This resemblance stems from a similar mass of metals in the CGM of both simulations. While KI has a large gas reservoir at low metallicity, KR has a small gas mass at high metallicity. KI and KR are also comparable in C IV and O VI. Now comparing KI and KR to DC, we find that DC has higher column densities in both C IV and O VI, thanks to a high gas mass with high metallicity in the CGM, and thus a higher CGM metal mass in the CGM. A second important conclusion from this figure is the comparison between simulations and observations. While all simulations fail to match observations in Mg II, DC shows the best agreement with observations of C IV and O VI.

4 Conclusions

We perform three RAMSES-RT cosmological zoom simulations of the same galaxy with three subgrid models commonly used in the literature: KI, KR and DC. We first calibrate our simulations in stellar mass at $z = 1$ and find that the three models still lead to different CGM properties, with KI and DC exhibiting high CGM gas mass, and KR and DC showing high CGM metallicity. We then post-process our simulations with KROME and RASCAS to compute H I, Mg II, C IV, and O VI column densities and find that CGM column densities are a potent tool to discriminate degenerate feedback models. It is necessary to compare them with complementary observables, i.e. both non-metallicity-dependent elements (H I) and metallicity-dependent ions tracing different phases of the gas. When comparing simulations to observations, we find that all models fail to reproduce observables, except for DC, in better agreement with C IV, and O VI thanks to a higher CGM metal mass. Although limited by a small observational dataset, this study underscores the potential of quasar sightlines to improve subgrid models in numerical simulations.

The simulations presented here were run on the CCF (Common Computing Facility) of the LABEX Lyon Institute of Origins (ANR-10-LABX-0066) and the PSMN (Pôle Scientifique de Modélisation Numérique) of the ENS de Lyon. MR and TK are supported by the National Research Foundation of Korea (NRF) grant funded by the Korean government (Nos. 2020R1C1C1007079 and 2022R1A6A1A03053472).

References

Behroozi, P., Wechsler, R. H., Hearin, A. P., & Conroy, C. 2019, Monthly Notices of the Royal Astronomical Society, 488, 3143

Chang, Y.-L., Lan, T.-W., Prochaska, J. X., et al. 2024, Probing the Impact of Radio-Mode Feedback on the Properties of the Cool Circumgalactic Medium

Crain, R. A. & van de Voort, F. 2023, Annual Review of Astronomy and Astrophysics, 61, 473

Faucher-Giguère, C.-A. & Oh, S. P. 2023, Annual Review of Astronomy and Astrophysics, 61, 131

Genel, S., Bryan, G. L., Springel, V., et al. 2019, The Astrophysical Journal, 871, 21

Grassi, T., Bovino, S., Schleicher, D. R. G., et al. 2014, Monthly Notices of the Royal Astronomical Society, 439, 2386

Grevesse, N., Asplund, M., Sauval, A. J., & Scott, P. 2010, Astrophys Space Sci, 328, 179

Hahn, O. & Abel, T. 2011, Monthly Notices of the Royal Astronomical Society, 415, 2101

Keller, B. W., Wadsley, J. W., Wang, L., & Kruijssen, J. M. D. 2019, Monthly Notices of the Royal Astronomical Society, 482, 2244

Kimm, T., Katz, H., Haehnelt, M., et al. 2017, Monthly Notices of the Royal Astronomical Society, 466, 4826

Kretschmer, M. & Teyssier, R. 2020, Monthly Notices of the Royal Astronomical Society, 492, 1385

Mauerhofer, V. 2021, PhD thesis, Université de Lyon ; Université de Genève

Michel-Dansac, L., Blaizot, J., Garel, T., et al. 2020, Astronomy and Astrophysics, 635, A154

Moster, B. P., Naab, T., Lindström, M., & O'Leary, J. A. 2021, Monthly Notices of the Royal Astronomical Society, 507, 2115

Rosdahl, J. & Teyssier, R. 2015, Monthly Notices of the Royal Astronomical Society, 449, 4380

Teyssier, R. 2002, Astronomy and Astrophysics, 385, 337

Teyssier, R., Pontzen, A., Dubois, Y., & Read, J. I. 2013, Monthly Notices of the Royal Astronomical Society, 429, 3068

Vogelsberger, M., Marinacci, F., Torrey, P., & Puchwein, E. 2020, Nature Reviews Physics, 2, 42